Journal of Solid State Chemistry 190 (2012) 98–103

Contents lists available at SciVerse ScienceDirect

Journal of Solid State Chemistry

journal homepage: www.elsevier.com/locate/jssc

Controlled synthesis, formation mechanism and upconversion luminescence of $NaYF_4$: Yb, Er nano-/submicrocrystals via ionothermal approach

Jia Liu [a,c,1], Xiaomin Liu [a,1], Xiangui Kong [a,*], Hong Zhang [b]

[a] State Key Laboratory of Luminescence and Application, Changchun Institute of Optics, Fine Mechanics and Physics, Chinese Academy of Sciences, Changchun 130033, PR China
[b] Van't Hoff Institute for Molecular Sciences, University of Amsterdam, Science Park, PO Box 94157. 1090 GD Amsterdam, The Netherlands
[c] Graduate School of Chinese Academy of Sciences, Beijing 100039, PR China

ARTICLE INFO

Article history:
Received 9 October 2011
Received in revised form
6 December 2011
Accepted 29 January 2012
Available online 15 February 2012

Keywords:
Ionothermal
Rare earths
Crystal growth
Upconversion luminescence

ABSTRACT

In order to deepen the fundamental understanding of IL-mediated synthesis of nano-/submicrostructure, hydrophilic ILs ([Emim][BF_4], [Bmim][BF_4] and [Omim][BF_4]), which act as solvents, templates, as well as fluorine source, have been employed to synthesize rare earth doped $NaYF_4$ upconversion nano-/submicrocrystals (UC-NMCs). The imidazolium cations provide the capping reagent to prevent the nucleation centers from aggregation and growing, while the tetrafluoroborate anions introduce a new fluorine source according to partial hydrolysis. It is demonstrated that the properties of IL, such as viscosity, polarity, solvency and interfacial tension, extremely affect the dissolution, diffusion and nucleation process of lanthanide ions in IL. Morphology and size of the final products can thus be tailored by synthetical parameters, like imidazolium cations, cosolvents, Ln^{3+} and fluoride concentrations, as well as ionothermal time. Based on the experimental results, the possible mechanism of the nucleation and growth of UC-NMCs in IL is discussed.

1. Introduction

Room temperature ionic liquids (RTILs) are generally defined as salts with melting points below 100 °C [1]. Most of the investigated RTILs consist of 1-alkyl-3-methylimidazolium (abbreviated [C*n*mim]$^+$, where *n* is the number of carbon atoms in a linear alkyl chain). The cations are combined with either organic or inorganic anions. Because of their environmental benign and some unique properties, typically their structures resulting in tunable physical and chemical prosperities, make them attractive to synthesis, catalysis, separations, and electrochemistry [2]. Recently, the synthesis of inorganic nanostructures in IL media has attracted extensive attention. In comparison to traditional solvents, they have found many merits, including negligible vapor pressure, good thermal and chemical stability, extremely high ionic conductivity, wide electrochemical windows, extended hydrogen bonding, template providers, capping agents [3,4]. Different classes of inorganic nanomaterials have been prepared in IL, like metals, metal oxides, metal alloys, metal fluorides, and so on [5–7]. Thermal reactions using ionic liquids as reaction media are often termed as "ionothermal" to distinguish them from hydrothermal and solvothermal methods, which take place in a predominantly molecular solvent.

On the other hand, researches on rare earth ions doped upconversion nanocrystals have been boosted in last decades with expectation that these materials may play a critical role in solid-state lasers, optical storage, flat-panel displays, optical fiber-based telecommunications, and especially in biology/biomedicine [8–17]. Among them, *ARE*F_4 (*A*=alkali; *RE*=rare earth) is regarded as an ideal host matrix for UC phosphors [18,19]. Various synthetic approaches have been reported for preparing controllable $NaYF_4$ nanocrystals [20,21]. The most adopted method to prepare $NaYF_4$ is co-thermolysis of trifluoroacetate precursors at high temperature [22–24]. Zhao et al. reported $NaYF_4$ nanotubes via an ion exchange procedure from the corresponding hydroxides [25]. Van Veggel's group developed an efficient route to prepare a UC nanoparticle-polymer composite [26]. Li et al. obtained morphology-controllable $NaYF_4$ nanocrystals hydrothermally/solvothermally using distilled water, acetic acid, or ethanol as the solvent [27]. Recently, IL was also applied to synthesize $NaYF_4$ UC nanophosphors [28]. Our group has successfully prepared the water-soluble pure hexagonal-phase nanoparticles in [Bmim][BF_4] [29]. From this aspect an illustration of the effect of the unique properties of ILs, especially their high polarity and viscosity, which largely affect the inorganic salts dissolving and diffusing ability, on the final product is very demanding. In addition, the effect of different ILs on the formation process of the nanostructures is also need to be explored.

* Corresponding author.
E-mail addresses: xgkong14@ciomp.ac.cn (X. Kong), h.zhang@uva.nl (H. Zhang).
[1] These authors contribute equally to this work.

0022-4596/$ - see front matter © 2012 Elsevier Inc. All rights reserved.
doi:10.1016/j.jssc.2012.01.058

In this work, many kinds of hydrophilic ILs ([Emim][BF_4], [Bmim][BF_4] and [Omim][BF_4]), which act as solvents and templates, as well as fluorine source [30–32], have been employed to synthesize rare earth ions doped luminescence upconversion nano-/submicrocrystals. Through the manipulation of a series of experimental conditions in ILs, such as kinds of imidazolium cations, volumes of cosolvent, concentrations of Ln^{3+} (Ln=Y, Yb and Er) and fluoride, as well as ionothermal time, we adjusted the dissolution, diffusion and nucleation rate of the rare earth ions in ILs and then successfully obtained different morphologies and sizes of the final products. Based on the experimental results, the possible mechanism of the nucleation and growth of UC-NMCs in ILs is concluded, which strengthens the fundamental understanding of IL-mediated synthesis of nano-/submicrostructure.

2. Experimental section

2.1. Materials

All reagents were analytical grade. $Ln(NO_3)_3 \cdot 6H_2O$ salt was purchased from Beijing Chemical Plant (Beijing, China). [Emim][BF_4], [Bmim][BF_4] and [Omim][BF_4] were purchased from Shanghai Chengjie Chemical Co., Ltd., China (97%). These chemicals were used without further purification.

2.2. Synthesis of $NaYF_4$: Yb^{3+}, Er^{3+} phosphors

In a typical synthetic procedure for the preparation of $NaYF_4$: 20 mol% Yb^{3+}, 2 mol% Er^{3+} phosphors, a certain amount of $Ln(NO_3)_3 \cdot 6H_2O$ (lanthanide ion molar ratio, Y/Yb/Er=78:20:2) and 0.056 g NaCl were added into a beaker containing ILs and stirred for 30 min at 80 °C, the above mixed solution was then transferred into a 23 mL Teflon-lined autoclave and heated at the elevated temperature for several hours, before being cooled to room temperature and diluted with the appropriate absolute ethanol or acetone. Finally, the precipitates were collected through centrifugation at a speed of 6000 rpm, washed by absolute ethanol, and dried in vacuum at 50 °C. Samples with other synthetical parameters were prepared in a similar way (see Supporting Information for the complete synthetic approaches).

2.3. Characterization

The structure and morphology of $NaYF_4$: Yb^{3+}, Er^{3+} UP-NMCs were characterized by XRD using a Bruvker D8-advance X-ray diffraction with Cu K_α radiation (λ=1.5418 Å), and field emission scanning electron microscope (FESEM, Hitachi, S-4800). The upconversion emission spectra of $NaYF_4$: Yb^{3+}, Er^{3+} UP-NMCs were acquired using a Jobin-Yvon LabRam Raman spectrometer system equipped respectively with 1800 and 600 grooves/mm holographic gratings, respectively, and a Peltier air-cooled CCD detector. The samples were excited by a CW semiconductor diode laser at 980 nm. The maximal excitation power used in the experiment was about 760 mW with a focusing area of about 0.03 mm^2. The upconversion luminescence spectra were measured under identical conditions in order to compare their relative emission intensities.

3. Results and discussion

First of all we demonstrate the feasibility of using ILs to synthesize $NaYF_4$ nanocrystals. Regarding the selection of ILs, we focus on the hydrophilic dialkylimidazolium tetrafluoroborate-based compounds, such as [Emim][BF_4], [Bmim][BF_4] and [Omim][BF_4]. The imidazolium cations provide the capping reagent for preventing the $NaYF_4$ nucleation centers from aggregation and growing, whereas the tetrafluoroborate anions introduce a new fluorine source according to partial hydrolysis. Therefore, such ILs can act as solvents, reaction agents and templates. Furthermore, the alkyl chain on an imidazole ring greatly affects the physical and chemical properties of dialkylimidazolium-based ILs, such as melting point, viscosities, polarity, solvency and interfacial tension, which directly influence the dissolution, diffusion and nucleation process of the lanthanide ions in ILs. Consequently, we can tailor the morphology and size of the final product via altering the characteristics of the IL. As a proof of concept, we have prepared the products obtained in several ILs. Fig. 1 displays the SEM images of $NaYF_4$: Yb^{3+}, Er^{3+} nanocrystals synthesized in [Emim][BF_4], [Bmim][BF_4] and [Omim][BF_4] under the same synthesis conditions. Compared with these three ILs, they have the same anion $[BF_4]^-$ but different length of alkyl chains on the imidazole ring, which contribute mainly to their diverse properties, such as melting point, viscosity, interface tension as listed in Table 1. With the increasing of the length of the alkyl chains, the average size of the nanocrystals decreases from 70 to 35 nm and the morphology changes from grainy to spherical. It seems that the IL, [Omim][BF_4], possessing longer alkyl chain of the cation is in favor of small and isotropic nanocrystals. This is probably because that viscosity of an IL increases with alkyl chains lengthening, slowing down the dissolution and diffusion rate of the lanthanide ions in the IL. In addition, the longer the alkyl chains are, the weaker the interfacial tension will be, and consequently the nucleation process will become faster. A slow dissolution and diffusion, and fast nucleation process is easier to obtain UC nanocrystals with small size.

Considering the advantage of [Omim][BF_4] in obtaining small and isotropic UC nanocrystals, we have focused on this kind of IL to study the ionothermal method in detail. The synthetic conditions and corresponding characteristics of samples prepared via the ionothermal route are summarized in Table 2. The optimal synthetic parameters for uniform, hexagonal phase nanoparticles

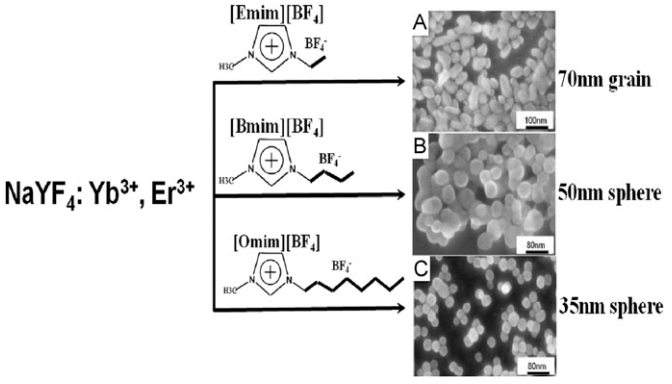

Fig. 1. Schematic representation of the formation of $NaYF_4$ nacocrystals obtained in different ILs.

Table 1
Different properties of these three ILs ([Emim][BF_4], [Bmim][BF_4] and [Omim][BF_4]).

Title	Mp (°C)	Viscosity (cP)	Interface tension (mJ m^{-2})
[Emim][BF_4]	15	153	50.4
[Bmim][BF_4]	25	233	43.9
[Omim][BF_4]	28	422	32.5

Table 2
Synthetic conditions and characteristics of the samples prepared via ionothermal approach.

Sample	The volume of the cosolvent (mL)	Ln^{3+}/F^{-}/NaCl molar ratio	Ionothermal time (h)	Ionothermal temperature (°C)	Morphology	Reference
1	0	1:4:1	10	180	Sphere	Fig. 2A
2	0	1:6:1	10	180	Sphere	Fig. 2B
3	0	1:8:1	10	180	Sphere	Fig. 2C
4	0	1.5:8:1	10	180	Sphere	Fig. 4B
5	0	2:8:1	10	180	Rod	Fig. 4C
6	0	1:8:1	14	180	Sphere	Fig. 5B
7	0	1:8:1	18	180	Spindle	Fig. 5C
8	0	1:8:1	22	180	Plates	Fig. 5D
9	0.5	1:8:1	10	180	Sphere	Fig. 6A
10	1	1:8:1	10	180	Sphere/flower	Fig. 6B
11	2	1:8:1	10	180	Flower	Fig. 6C
12	0	1:8:1	10	140	Amorphous	Fig. S1A
13	0	1:8:1	10	160	Amorphous	Fig. S1B

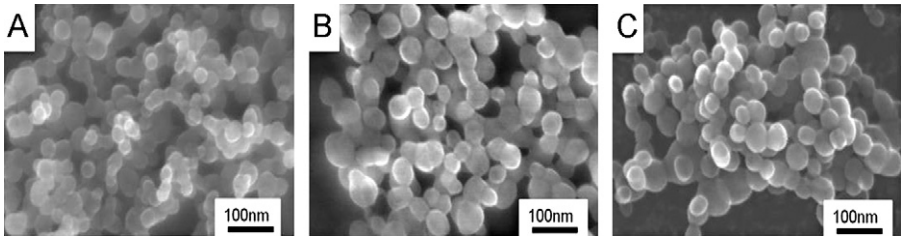

Fig. 2. SEM images of the $NaYF_4$: Yb^{3+}, Er^{3+} nanocrystals obtained with different F^{-}/Na^{+} ratios: (A) $F^{-}:Na^{+}=4:1$; (B) $F^{-}:Na^{+}=6:1$; (C) $F^{-}:Na^{+}=8:1$.

(Sample 3) are found, i.e., a molar ratio of Ln^{3+}/F^{-}/NaCl of approximately 1:8:1 and an ionothermal time of 10 h at a temperature of 180 °C. For submicrorods (Sample 5), the optimal parameters are: molar ratio of Ln^{3+}/F^{-}/NaCl of approximately 2:8:1, ionothermal time of 10 h at 180 °C. In addition, for pure hexagonal $NaYF_4$ submicroplates (Sample 8), the optimal parameters are as follows: molar ratio of Ln^{3+}/F^{-}/NaCl of approximately 1:8:1, ionothermal time of 22 h at a temperature of 180 °C. As is manifested in the experiments, Ln^{3+} and fluoride concentrations, ionothermal time, as well as viscosity are the key factors for the crystal structure, morphology and size of the final products.

3.1. *Effect of the $[BF_4]^{-}$ concentration*

IL acts as fluorine source in the way of fast hydrolysis of $[BF_4]^{-}$ anion in the presence of lanthanide nitrate with hydration water molecules. To investigate the effect of the F^{-} content on the morphology, size and structure of the as-prepared UC nanocrystals, the F^{-}/Na^{+} ratio was taken as 4, 6 and 8, respectively. The samples prepared with low F^{-} concentration, i.e., $F^{-}:Na^{+}=4:1$, are aggregates of many primary particles with a coarse surface (see Fig. 2(A)), indicating low crystallization of the sample [33]. When the F^{-} concentration increases, the nanoparticles grow up from 25 to 35 nm, and meanwhile, the crystallization of the $NaYF_4$ is improved, as evidenced by the smoother surface and more regular shape (see Fig. 2(C)). Furthermore, the crystal structure of the sample is also affected by the $[BF_4]^{-}$ concentration. Fig. 3 displays the corresponding XRD patterns of the final products prepared with different F^{-}/Na^{+} ratios. The bottom pattern depicted in Fig. 3(a) matches well with the standard cubic structure data, whereas the top XRD pattern shown in Fig. 3(c) coincides with the hexagonal phase $NaYF_4$. Therefore, the crystal structure undergoes transformation from the cubic phase to the hexagonal phase during ionothermal treatment with F^{-}/Na^{+} ratio increasing.

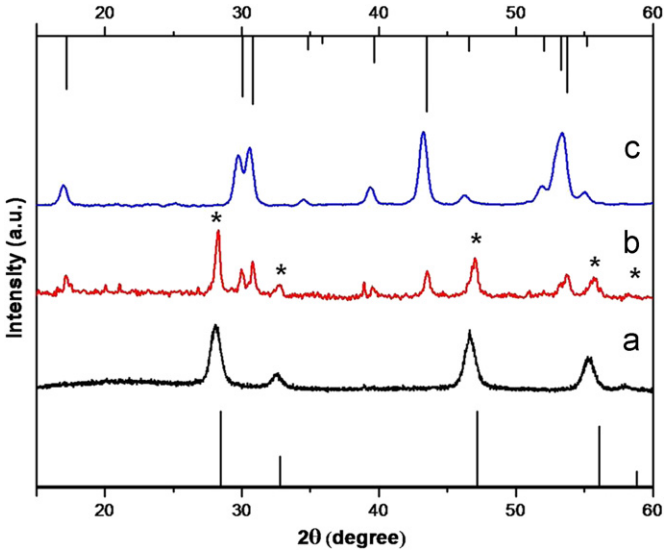

Fig. 3. XRD patterns of the $NaYF_4$: Yb^{3+}, Er^{3+} crystallites prepared with different F^{-}/Na^{+} ratios: (a) $F^{-}:Na^{+}=4:1$; (b) $F^{-}:Na^{+}=6:1$; (c) $F^{-}:Na^{+}=8:1$. The sign (*) represents the cubic phase.

It is well established that the hexagonal phase is a more ordered and thermodynamically stable phase and that the transition from cubic to hexagonal phase is a disorder-to-order character with respect to cations [34]. Thoma et al. reported that the temperature influences the phase change from cubic to hexagonal $NaYF_4$ [35]. This phase transition behavior can be controlled by changing the environment or the energy barrier [36,37]. Analysis suggests that the phase transformation from cubic to hexagonal phase is mainly due to the modification of the environment of Y^{3+} occupation sites, including coordination number [38,39]. Y^{3+} or other cationic sites are conveniently coordinated by F^{-} ions when increasing the fluoride concentration, which will decrease the energy barrier, and as a result, an ordered hexagonal structure appears at $F^{-}:Na^{+}=8:1$. However, a

less ordered cubic structure is obtained at F^-:Na^+=4:1. Therefore, fluoride concentration plays an important role in determining the crystal structure [40].

3.2. Effect of reactant Ln^{3+} concentration

The effects of the total amount of Ln^{3+} on morphologies and sizes of the products have been studied by changing the content of Ln^{3+}. When Ln^{3+}/Na^+ ratio is 1, the products are composed of spheres with mean diameter of 35 nm (Fig. 4(A)). When the ratio increases to 1.5, larger nanospheres are formed with the average size of 75 nm (Fig. 4(B)). However when the ratio reaches to 2, submicrorods of a length roughly equal to 1.6 μm and cross section diameter of 280 nm are obtained (Fig. 4(C)). These results indicate that the Ln^{3+} content can be used to control the size and morphology of the particles. Apparently, large amount of Ln^{3+} might augment the probability of lanthanide ions in dissolution and diffusion process, leading to the relatively large particles.

3.3. Effect of ionothermal time

It is expected that the ionothermal time also affects the growth of the UC nanocrystals, especially the morphologies of the nanocrystals. Under the same synthesis conditions, the reaction time is extended from 10 to 22 h by step of 4 h. The obtained UC-NMCs exhibit different morphologies including sphere, spindle and hexagonal plates (Fig. 5). As is shown in the figure, the samples are composed of nanoparticles with an average size of 35 nm when the ionothermal time lasts 10 h (Fig. 5(A)). Extending the ionothermal time to 14 h increases the size of the nanoparticles to 70 nm and at the same time the dispersity of the products become better (Fig. 5(B)). Interestingly, the morphologies of the sample change greatly when the inonthermal time extends to 18 h and 22 h. Spindle-shaped submicrocrystals with aspect ratio (length/breadth) of about 1.5 when the inonthermal time is 18 h (Fig. 5(C)). Further extending the reaction time to 22 h, pure hexagonal-shaped $NaYF_4$ submicroplates are formed with a side length of 300 nm and thickness of 350 nm (Fig. 5(D)). It seems that the long ionothermal time facilitates the growth of submicrocrystals, by supplying energy to speed up the dissolution and crystallization process, namely the Ostwald-ripening process [41].

3.4. Effect of volume of ethanol

To further prove that the polarity, viscosity and interfacial tension of the ILs affect the solvation, diffusion and nucleation process of the lanthanide ions in IL, ethanol was used as cosolvent to vary these properties of the IL. Ethanol here serves with three purposes: (1) to increase the polarity of solvent, which benefits the solvation of the lanthanide ions in the ILs, (2) to decrease the viscosity of the ILs, which speeds up the diffusion rate of the lanthanide ions and (3) to increase the interfacial tension to slow down the nucleation rate. Fig. 6 displays the SEM images of the final products obtained with different ethanol volumes. It is shown that the $NaYF_4$ nanocrystals prepared with ethanol volume of 0.5 mL have homogeneous sphere-like shape with an average size of 50 nm (Fig. 6(A)). Fig. 6(B) exhibits the morphology of the sample obtained with ethanol volume of 1 mL and other conditions keep the same as those in Fig. 6(A). It can be seen that the samples are composed of sphere-like nanocrystals and flower-like microcrystals which aggregate together. When ethanol volume is further increased to 2 mL, only aggregated flower-like microcrystals are obtained. We can thus conclude that low volume of ethanol favours the formation of small size nanoparticles, whereas high ethanol volume benefits the formation of mix-shaped crystals or submicroflowers. It is mainly because that cosolvent ethanol might decrease the viscosity of the IL and simultaneously increase its polarity, enhancing the solvency of reactant, resulting in the fast process of the dissolution and diffusion of the lanthanide ions in the IL. In addition, accompanied with the lower viscosity, the surface tension becomes larger, which leads to a strong Ostwald ripening process [42]. Thereby the products change from small size nanoparticles to submicroflowers.

3.5. Formation mechanism

Dissolution of Ln^{3+} in room-temperature ionic liquids has been well studied, especially by molecular dynamics simulation. Quantum calculation on the behavior of the lanthanide ions and ILs supports that when lanthanide nitrate were dispersed in ILs, the Ln^{3+} ions were surrounded first by the anions of ILs, and the first shell was surrounded by imidazolium cations. At the same time, the NO_3^- ions were surrounded by a rigid "cage" of imidazolium cations[43,44]. Based on these studies and the obtained experimental results, we can have an insight of nucleation and growth mechanism of UC-NMCs in an IL. When Ln^{3+} ions were dissolved in ILs like [Omim][BF_4], they were surrounded by the $[BF_4]^-$ anions, $[Omim]^+$ cations, Na^+ cations and NO_3^- ions. All the Ln^{3+} ions were in the same chemical environments. When the mixture was heated continuously, some

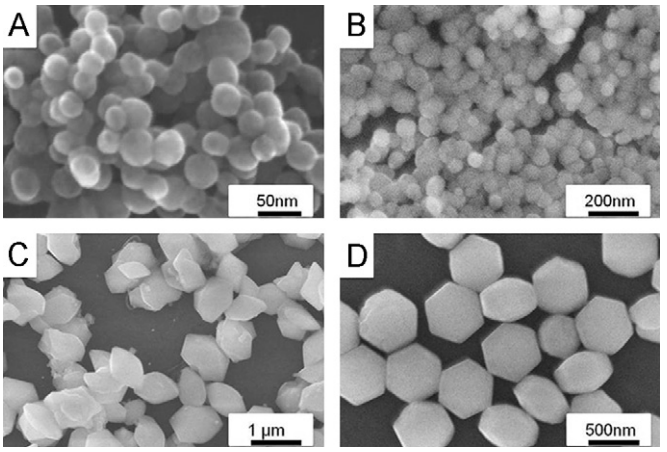

Fig. 5. SEM images of the $NaYF_4$: Yb^{3+}, Er^{3+} nanocrystals obtained with different ionothermal times: (A) 10 h; (B) 14 h; (C) 18 h; (D) 22 h.

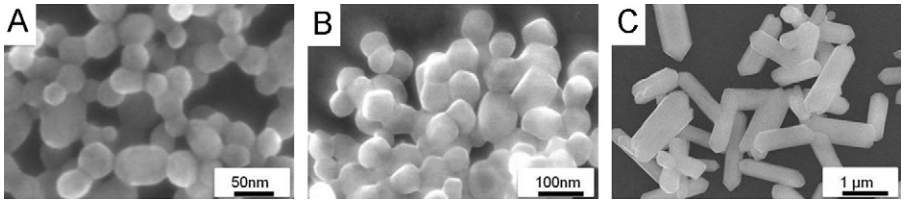

Fig. 4. SEM images of the $NaYF_4$: Yb^{3+}, Er^{3+} nanocrystals obtained by different reactant Ln^{3+} concentration: (A) Ln^{3+}:Na^+=1:1; (B) Ln^{3+}:Na^+=1.5:1; (C) Ln^{3+}:Na^+=2:1.

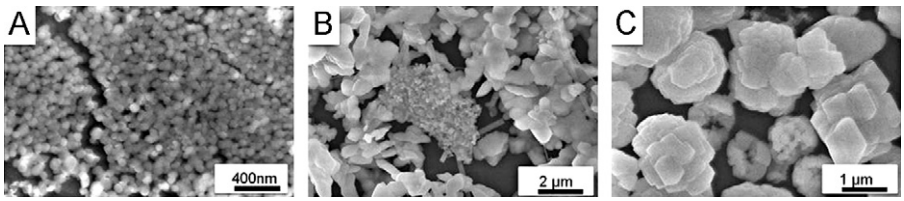

Fig. 6. SEM images of the $NaYF_4$: Yb^{3+}, Er^{3+} nanocrystals obtained in different ethanol volumes: (A) 0.5 mL; (B) 1 mL; (C) 2 mL (The total volume of the solvent was kept at 10 mL).

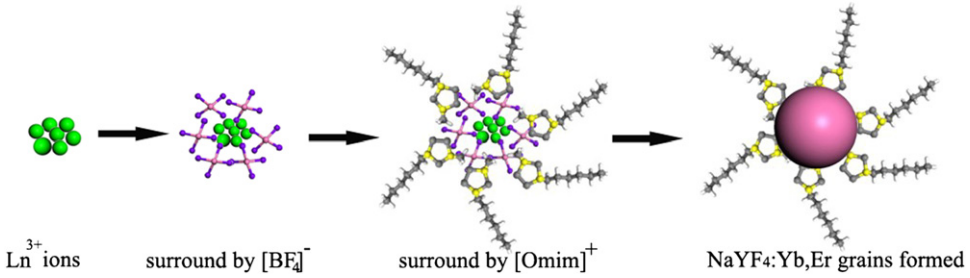

Fig. 7. Schematic illustration of a possible formation mechanism of $NaYF_4$ in ILs.

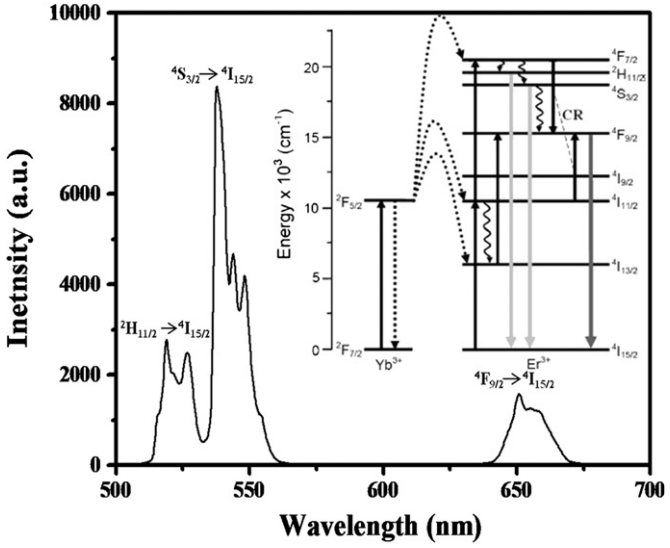

Fig. 8. Upconversion luminescence spectra of $NaYF_4$: 20 mol% Yb^{3+}, 2 mol% Er^{3+} upon irradiation at 980 nm. Inset: a schematic illustration of the upconversion luminescence processes of $NaYF_4$: Yb^{3+}, Er^{3+} crystals.

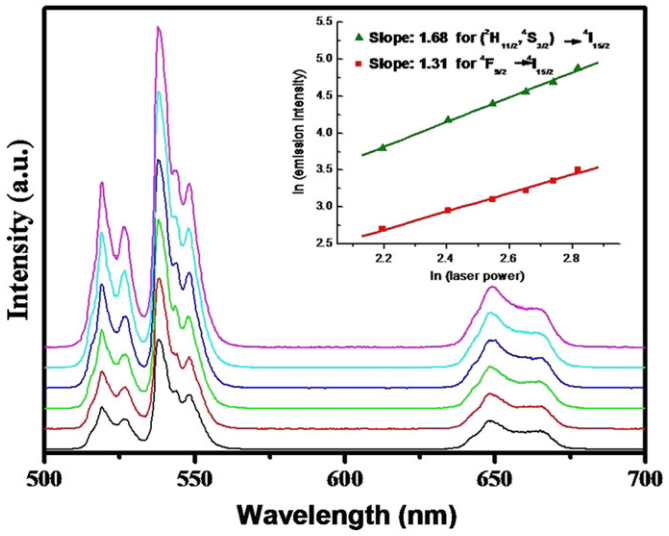

Fig. 9. Upconversion luminescence spectra of $NaYF_4$: 20 mol% Yb^{3+}, 2 mol% Er^{3+} upon irradiation at 980 nm under different pump power levels (sample 3). Inset: pump power dependence of the upconverted green and red integrated intensities.

$[BF_4]^-$ ions were degraded and brought F^-, leading to the formation of $NaYF_4$ grains. The ILs acted as a coordinating solution and the reaction in such a solvent was also similar to a reaction in pure "universal" ligands, which prevented the $NaYF_4$ nucleation centers from growing (see Fig. 7). Furthermore, the low interface tension of [Omim][BF_4] led to high nucleation rates, small particles could thus be generated which undergo Ostwald ripening weakly [45,46].

3.6. Upconversion luminescence properties

Upconversion luminescence processes of rare earth ions doped in solid materials have been widely investigated [47,48]. Fig. 8 shows the upconversion emission spectra of 1 wt% solution of $NaYF_4$: 20 mol% Yb^{3+}, 2 mol% Er^{3+} nanocrystal (Sample 3). Upconverted emission is observed in the green and red spectral regions following continuous wave (CW) excitation with 980 nm NIR radiation. Green emissions are observed in the 510–530 nm and 530–570 nm regions, assigning to the $^2H_{11/2}$ and $^4S_{3/2}$ excited states to the $^4I_{15/2}$ ground state transitions. Furthermore, a red emission in the 635–675 nm regions is assigned to the $^4F_{9/2}$ excited state to the $^4I_{15/2}$ ground state. In order to further investigate the upconversion luminescence mechanism, the pump power dependent luminescence intensity was also performed. It is well-known that $I_{em} \propto I_P^n$ exists in upconversion processes, where n denotes the number of NIR photons absorbed to generate one frequency upconverted photon [49]. The pump power dependence is exemplified in Fig. 9, fitting the data points yielded approximately slopes of 1.68 and 1.31 for the ($^2H_{11/2}$, $^4S_{3/2}$)→$^4I_{15/2}$ and $^4F_{9/2}$→$^4I_{15/2}$ transitions, respectively, indicating the upconversion luminescence involves a two-photon absorption process. The results further support the energy-transfer and upconversion emission process of the final products. It is proved that the ionothermal approach do not change the upconversion properties of the as-prepared UP-NMCs.

4. Conclusions

Upconversion nano-/submicrocrystals were successfully obtained with different morphologies and sizes via ionothermal method. The effect of the properties of ILs, such as viscosities, polarity, solvency and interfacial tension on the morphology and size of the product was studied and highlighted. The underlying mechanism was explored. Since the IL-based approach is efficient and environmental benign, we believe this method would offer an interesting opportunity in the fabrication of nanocrystals and also extent the application of ILs in nanochemistry.

Acknowledgments

This work was financially supported by the exchange program between the Academy of Sciences of China and the Royal Netherlands Academy of Sciences of the Netherlands, and the National Natural Science Foundation of China (Grant No 11174277, 11004189 and 10904142).

Appendix A. Supporting materials

Supplementary data associated with this article can be found in the online version at doi:10.1016/j.jssc.2012.01.058.

References

[1] P. Hapiot, C. Lagrost, Chem. Rev. 108 (2008) 2238–2264.
[2] V.I. Parvulescu, C. Hardacre, Chem. Rev. 107 (2007) 2615–2665.
[3] F. Endres, Chem. Phys. Chem. 3 (2002) 144–154.
[4] H.X. Gao, J.C. Li, B.X. Han, W.N. Chen, J.L. Zhang, R. Zhang, D.D. Yan, Phys. Chem. Chem. Phys. 6 (2004) 2914–2916.
[5] K. Biswas, C.N.R. Rao, Chem. Eur. J. 13 (2007) 6123–6129.
[6] T. Kameyama, Y. Ohno, T. Kurimoto, K. Okazaki, T. Uematsu, S. Kuwabata, T. Torimoto, Phys. Chem. Chem. Phys. 12 (2010) 1804–1811.
[7] E. Redel, M. Walter, R. Thomann, L. Hussein, M. Krüger, C. Janiak, Chem. Commun. 46 (2010) 1159–1161.
[8] D.K. Chatterjee, A.J. Rufaihah, Y. Zhang, Biomaterials 29 (2008) 937–943.
[9] L.Q. Xiong, T.S. Yang, Y. Yang, C.J. Xu, F.Y. Li, Biomaterials 31 (2010) 7078–7085.
[10] R. Kumar, M. Nyk, T.Y. Ohulchanskyy, C.A. Flask, P.N. Prasad, Adv. Funct. Mater. 19 (2009) 853–859.
[11] J. Shen, L.D. Sun, C.H. Yan, Dalton Trans. 42 (2008) 5687–5697.
[12] F. Wang, D. Banerjee, Y.S. Liu, X.Y. Chen, X.G. Liu, Analyst 135 (2010) 1839–1854.
[13] M. Kumar, P. Zhang, Biosens. Bioelectron. 25 (2010) 2431–2435.
[14] D.E. Achatz, R. Ali, O.S. Wolfbeis, Top. Curr. Chem. 300 (2011) 29–50.
[15] C.J. Carling, F. Nourmohammadian, J.C. Boyer, N.R. Branda, Angew. Chem. Int. Ed. 49 (2010) 3782–3785.
[16] G.F. Wang, Q. Peng, Y.D. Li, Chem. Eur. J. 16 (2010) 4923–4931.
[17] G.B. Shan, G.P. Demopoulos, Adv. Mater. 22 (2010) 4373–4377.
[18] G.S. Yi, G.M. Chow, Adv. Funct. Mater. 16 (2006) 2324–2329.
[19] H. Schafer, P. Ptacek, K. Kompe, M. Haase, Chem. Mater. 19 (2007) 1396–1400.
[20] F. Zhang, J. Li, J. Shan, L. Xu, D.Y. Zhao, Chem. Eur. J. 15 (2009) 11010–11019.
[21] J.W. Zhao, X.M. Liu, D. Cui, Y.J. Sun, Y. Yu, Y.F. Yang, C. Du, Y. Wang, K. Song, K. Liu, S.Z. Lu, X.G. Kong, H. Zhang, Eur. J. Inorg. Chem. (2010) 1813–1819.
[22] G.S. Yi, G.M. Chow, Chem. Mater. 19 (2007) 341–343.
[23] F. Vetrone, R. Naccache, V. Mahalingam, C.G. Morgan, J.A. Capobianco, Adv. Funct. Mater. 19 (2009) 2924–2929.
[24] O. Ehlert, R. Thomann, M. Darbandi, T. Nann, ACS Nano 2 (2008) 120–124.
[25] F. Zhang, D.Y. Zhao, ACS Nano 3 (2009) 159–164.
[26] J.C. Boyer, N.J.J. Johnson, F.C.J.M. van Veggel, Chem. Mater. 21 (2009) 2010–2012.
[27] X. Wang, J. Zhuang, Q. Peng, Y.D. Li, Nature 437 (2005) 121–124.
[28] C. Chen, L.D. Sun, Z.X. Li, L.L. Li, J. Zhang, Y.W. Zhang, C.H. Yan, Langmuir 26 (2010) 8797–8803.
[29] X.M. Liu, J.W. Zhao, Y.J. Sun, K. Song, Y. Yu, C. Du, X.G. Kong, H. Zhang, Chem. Commun. 43 (2009) 6628–6630.
[30] T.W. Wang, H. Kaper, M. Antonietti, B. Smarsly, Langmuir 23 (2007) 1489–1495.
[31] H.S. Park, S.H. Yang, Y.S. Jun, W.H. Hong, J.K. Kang, Chem. Mater. 19 (2007) 535–542.
[32] C. Zhang, J. Chen, Y.C. Zhou, D.Q. Li, J. Phys. Chem. C 112 (2008) 10083–10088.
[33] Y.J. Sun, Y. Chen, L.J. Tian, Y. Yu, X.G. Kong, J.W. Zhao, H. Zhang, Nanotechnology 18 (2007) 275609.
[34] Y. Wei, F.Q. Lu, X.R. Zhang, D.P. Chen, Chem. Mater. 18 (2006) 5733–5737.
[35] R.E. Thoma, H. Insley, G.M. Hebert, Inorg. Chem. 5 (1966) 1222–1229.
[36] J. Shan, Y. Ju, Nanotechnology 20 (2009) 275603.
[37] H.X. Mai, Y.W. Zhang, R. Si, Z.G. Yan, L.D. Sun, L.P. You, C.H. Yan, J. Am. Chem. Soc. 128 (2006) 6426–6436.
[38] N. Martin, P. Boutinaud, M. Malinowski, R. Mahiou, J.C. Cousseins, J. Alloys Compd. 275 (1998) 304–306.
[39] M.D. Mathews, B.R. Ambekar, A.K. Tyagi, J. Köhler, J. Alloys Compd. 377 (2004) 162–166.
[40] P. Ghosh, A. Patra, J. Phys. Chem. C 112 (2008) 3223–3231.
[41] J.W. Zhao, Y.J. Sun, X.G. Kong, L.J. Tian, Y. Wang, L.P. Tu, J.L. Zhao, H. Zhang, J. Phys. Chem. B 112 (2008) 15666–15672.
[42] P.W. Voorhees, J. Stat. Phys. 38 (1985) 231–252.
[43] A. Chaumont, G. Wipff, Phys. Chem. Chem. Phys. 7 (2005) 1926–1932.
[44] A. Chaumont, G. Wipff, Phys. Chem. Chem. Phys. 5 (2003) 3481–3488.
[45] M. Antonietti, D. Kuang, B. Smarsly, Y. Zhou, Angew. Chem. Int. Ed. 43 (2004) 4988–4992.
[46] C. Zhang, J. Chen, Chem. Commun. 46 (2010) 592–594.
[47] F. Auzel, Chem. Rev. 104 (2004) 139–173.
[48] P.S. Golding, S.D. Jackson, T.A. King, M. Pollnau, Phys. Rev. B 62 (2000) 856–864.
[49] G.Y. Chen, T.Y. Ohulchanskyy, R. Kumar, H. Agren, P.N. Prasad, ACS Nano 4 (2010) 3163–3168.